Polarization domain walls in optical fibres as topological bits for data transmission

M. Gilles[1], P.-Y. Bony[1], J. Garnier[2], A. Picozzi[1], M. Guasoni[1,3] and J. Fatome[1]*

Domain walls are topological defects that occur at symmetry-breaking phase transitions. Although domain walls have been intensively studied in ferromagnetic materials, where they nucleate at the boundary of neighbouring regions of oppositely aligned magnetic dipoles, their equivalents in optics have not been fully explored so far. Here, we experimentally demonstrate the existence of a universal class of polarization domain walls in the form of localized polarization knots in conventional optical fibres. We exploit their binding properties for optical data transmission beyond the Kerr limits of normally dispersive fibres. In particular, we demonstrate how trapping energy in a well-defined train of polarization domain walls allows undistorted propagation of polarization knots at a rate of 28 GHz along a 10 km length of normally dispersive optical fibre. These results constitute the first experimental observation of kink–antikink solitary wave propagation in nonlinear fibre optics.

A domain wall (DW) is a type of topological defect that connects two stable states of a physical system. DWs are known to form as a result of a spontaneous symmetry-breaking phase transition in a variety of contexts, among which the most common are magnetism[1], condensed matter[2], spinor Bose–Einstein condensates[3], biological physics (energy transfer in proteins and DNA fluctuations, deoxyribonucleic acid)[2], or particle physics and string theory[4]. They also appear as kinks, in close analogy with the celebrated kink solutions of the Sine–Gordon equation[2]. DW structures have been widely studied in ferromagnetic materials[1], in which they are known to bind regions in which all spins or magnetic dipoles are aligned in different directions[1,2,5–8]. Their unique properties are exploited in modern spintronic devices to store or transfer information[9–12]. Despite the fact that DWs have been the subject of numerous studies in ferromagnetism, it is important to note that their equivalents in optics have been poorly exploited so far.

Originally, optical DWs referred to vectorial structures that had been predicted theoretically in the defocusing regime of an isotropic single-mode fibre more than 20 years ago[13–16]. They are fundamentally related to the Berkhoer and Zakharov modulational instability phenomenon[17]. The DW corresponds to a localized structure of the kink type that connects two regions of space with different polarizations. In the transition region, the electromagnetic field switches between two stable states with orthogonal circular polarizations (note that in optical fibres the dynamics is purely temporal and the time along a pulse plays the role of the spatial variable). In this framework, the fast polarization knots lead to two anticorrelated coupled twin waves, where the strong binding force imposed by the cross-phase interaction can compensate for linear and nonlinear impairments induced by normal chromatic dispersion and self-phase modulation, respectively[16]. The polarization distribution is then locked along the propagation within well-defined and robust temporal regions interconnected by polarization DWs (PDWs)[14].

Owing to their topological nature, a transmission system based on PDWs simply relies on fast polarization switching along the domain edges. As a result, the domains of polarization can be of any time duration and thus can be encoded individually to carry optical data[18–20].

At variance with classical bright scalar solitons[21], the topological nature of PDWs makes them strongly robust with respect to external perturbations such as temporal or amplitude fluctuations[13,19]. This property is fundamentally linked to their topological nature, featuring an energy (Hamiltonian) minimum at both sides of the kink. Therefore, their robustness and attractive properties could find numerous applications in optical communications, all-optical processing, data storage and fibre laser devices. However, so far, PDWs remain essentially unexplored experimentally.

In 1999, Kockaert et al. experimentally investigated the vectorial modulational instability process in a small 1 m piece of isotropic fibre and reported an indirect observation of anticorrelated polarization dynamics[22,23], thus validating the theoretical predictions of Berkhoer and Zakharov. In a different context, antiphase behaviour on a nanosecond scale has been reported in fibre ring laser cavities[24,25] and interpreted recently in terms of PDW-like temporal structures[26,27]. Similar antiphase polarization switching has also been observed by Marconi and co-workers in a vertical-cavity surface-emitting laser[28], which revealed a novel form of dissipative cavity soliton[28,29]. It is important to remember that PDWs reported in laser systems refer to a completely different physics: an optical cavity is inherently a dissipative system[30], which is a marked distinction from the conservative system considered here.

In contrast to previous works, here we report the first direct observation of PDWs in the classical optical fibres commonly used in optical communications. From a broader perspective, it is found that modern conventional fibres exhibit previously unrevealed peculiar properties, which are shown to support the existence of PDWs in any arbitrary polarization basis. For this reason, the novel class of polarization structures reported here has been termed as universal PDW. More specifically, we provide a genuine demonstration of the existence of these fundamental structures and exploit their unique topological properties for optical data transmission beyond the nonlinear Kerr-induced limitations of classical normally dispersive fibres. More unexpectedly, we also highlight the robust attraction properties of these entities, manifested as the spontaneous emergence of synchronized PDWs from a system of incoherent random waves, leading to a phenomenon

[1]Laboratoire Interdisciplinaire Carnot de Bourgogne (ICB), UMR 6303 CNRS - Université de Bourgogne Franche-Comté, 9 Avenue Alain Savary, BP 47870, 21078 Dijon, France. [2]Laboratoire de Probabilités et Modèles Aléatoires, University of Paris VII, 75251 Paris, France. [3]Optoelectronics Research Centre, University of Southampton, Southampton SO17 1BJ, UK. *e-mail: jfatome@u-bourgogne.fr
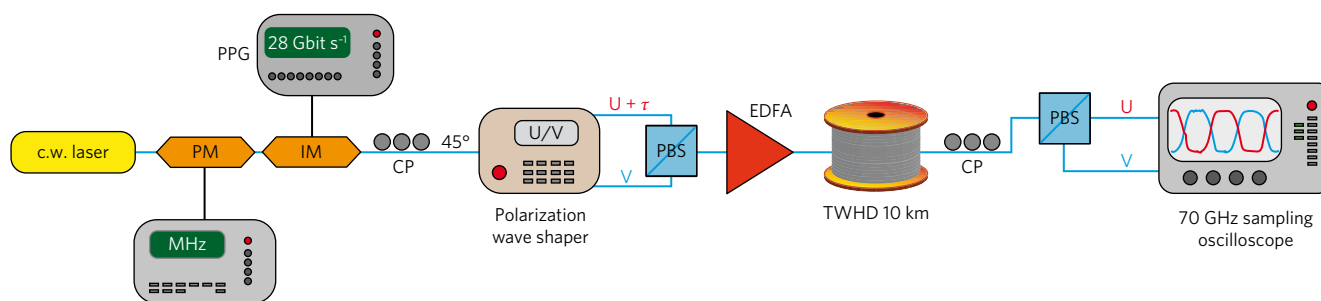
Figure 1 | Experimental set-up. To generate PDWs, a continuous-wave laser (c.w.) is first phase-modulated (PM) to enlarge its spectral linewidth and avoid any Brillouin backscattering within the fibre. Super-Gaussian pulses are then generated by means of an intensity modulator (IM) driven by a 28 Gbit s^{-1} pulse-pattern generator (PPG). The train of square-shaped pulses is then divided into two replicas, delayed by half a period (τ) and then orthogonally recombined by a polarization beamsplitter (PBS). The resulting signal consists of a train of 28 GHz polarization knots, which confine the energy in well-defined polarization regions. PDWs are amplified by an erbium-doped fibre amplifier (EDFA) and injected into a 10 km length of TrueWave high-dispersion fibre (TWHD). At the output of the system, both orthogonal polarization components are characterized in the time domain by a dual-input sampling oscilloscope. CP, polarization controller.

of polarization segregation, in analogy with the fundamental order–disorder phase transition in ferromagnetic materials. Finally, the present observation of PDWs in standard optical fibres raises important questions concerning the limits of the validity of the Manakov model for modern standard optical fibres, and opens new horizons for the development of isotropic data transmission.

Observation of PDW solitons

To demonstrate the robustness of PDWs following propagation in standard optical fibres, we used the experimental set-up shown in Fig. 1 (see Methods for details). An external cavity laser emitting at $\lambda = 1,555$ nm is phase-modulated to enlarge its spectral linewidth to prevent any Brillouin backscattering in the fibre under test. A train of super-Gaussian-shaped pulses is generated using an intensity Mach–Zehnder modulator driven by a 28 Gbit s^{-1} pulse-pattern generator (PPG) delivering simple periodic 0–1 switching. The resulting signal consists of a train of 30 ps square-shaped pulses at a repetition rate of 14 GHz (duty cycle of 1:2). The signal is then divided into two replicas; one is accurately delayed by a half period, and they are then orthogonally recombined by a polarization beamsplitter (PBS). Both delayed orthogonal replicas are thus anticorrelated and consist of a train of 28 GHz polarization knots, confining the energy in well-defined polarization domains. Note that the corresponding total intensity profile remains almost constant. After amplification by an erbium-doped fibre amplifier (EDFA), the PDWs are injected into a 10-km-long standard TrueWave fibre characterized by a normal chromatic dispersion $D = -14.5$ ps nm^{-1} km^{-1} at 1,550 nm and a nonlinear Kerr coefficient $\gamma = 2.5$ W^{-1} km^{-1}. It is important to stress that the fibre under test is non-isotropic. It is equivalent to a commercially available telecom fibre and therefore exhibits a randomly distributed residual birefringence, as well as an imposed birefringence spinning aimed at controlling such natural birefringence fluctuations (see Methods and Supplementary Section II.A). Moreover, in the present experiment, the input polarization basis can be selected arbitrarily, which makes our PDWs universal. Indeed, this behaviour is in huge contrast to the isotropic fibre case, for which circular polarizations are a prerequisite for the formation of DWs[16]. Finally, after transmission through the fibre, both orthogonal polarization components are characterized in the time domain thanks to a second PBS and a dual-input 70 GHz bandwidth sampling oscilloscope.

Figure 2a illustrates the signal monitored at the output of the 10-km-long fibre as a function of injected power when only one polarization component of the domains is injected. Due to the combined effects of chromatic dispersion and self-phase modulation, the output signal deteriorates rapidly into a complex periodic pattern, which subsequently leads to the development of the

shock-wave (wave breaking) singularities inherent to the defocusing regime considered here[31–33]. In contrast, as shown in Fig. 2b, when both orthogonally polarized twin waves are injected into the fibre, the cross-phase modulation interlocks the two signals in a symbiotic fashion[34]. In fact, like a chain of particles trapped in a periodic potential, the energy contained in each domain is confined due to the perfect balance between chromatic dispersion, self-phase modulation and cross-phase modulation occurring at the domain interfaces. Moreover, it is interesting to notice that to maintain such a balance between nonlinear and dispersive effects, an increase in the injected power leads to a reduction in the transition (rising and falling) time between adjacent PDW domains. This also reveals that dispersion plays a key role in DW structures, making them of a different nature to those studied in the backward wave configuration[35]. As shown in Fig. 2c, for an input power of 26 dBm, the output intensity profiles recorded on each polarization component of a domain (red and blue solid lines) remain undistorted compared to the input conditions (in stars), demonstrating the strength of the kink-based DW solitons in the presence of propagation impairments. Indeed, when a single component propagates (with half the total power, pink dashed line), the output intensity profile no longer fits the initial kink-shaped transition, confirming the high level of impairments induced by the nonlinear scalar transmission. We also stress the excellent agreement between the experimental measurements, the numerical simulations including experimental parameters (triangles), and the predicted PDW profile (circles; see Methods). Note that similar results have been obtained for different choices of input polarization basis.

To further assess the quality of the transmitted intensity profiles, we computed the correlation between the initial and output signals as a function of injected power. Intuitively, the correlation factor ρ is a number between zero and unity that denotes the level of statistical resemblance between the intensity fluctuations of the input and output waves (see Methods for the definition of ρ). As shown in Fig. 2d, the single-component configuration (circles) is characterized by a fast decrease of the correlation function, underlying a dramatic degradation of the propagating wave. In contrast, the robustness of the PDWs (red triangles) allows the correlation factor to be maintained, and even improve to nearly 1, thus revealing a high fidelity of the transmitted kinks and antikinks. This clearly confirms the stability and robustness of the propagating polarization domains.

Data transmission through PDWs

To confirm that the system propagates genuine kink solitons, we assessed the capability of PDWs to transmit optical data. Indeed, because DWs are solely defined as fast localized polarization
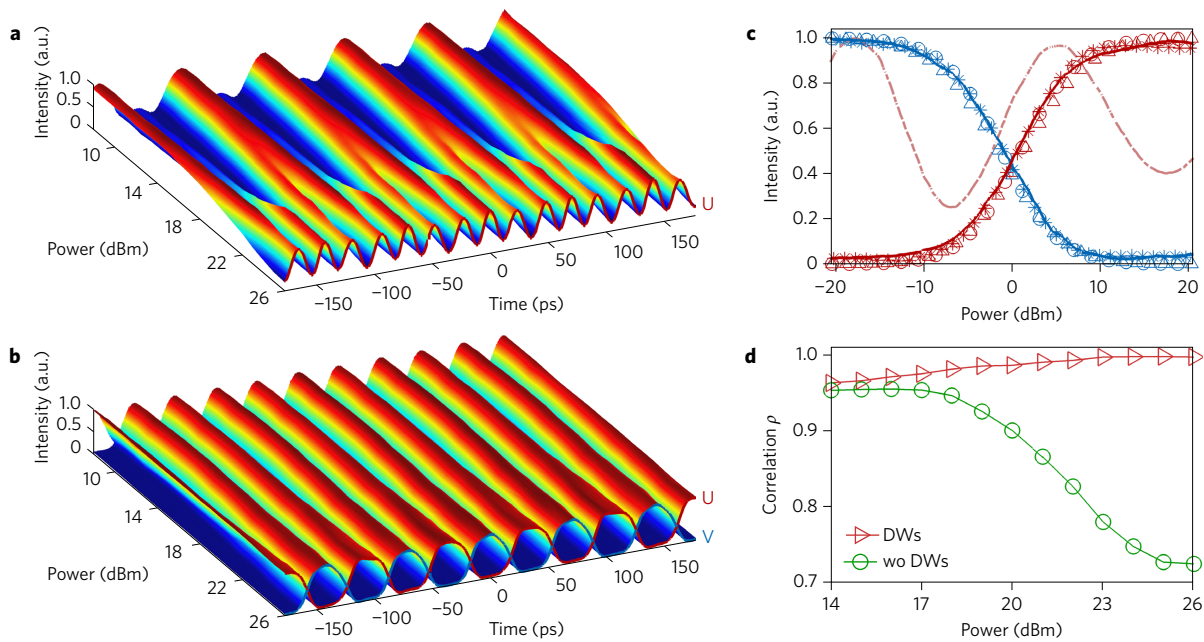
Figure 2 | Experimental observation of polarization domain wall (PDW) solitons. a,b, False-colour plot showing the evolution of the output intensity profile with injected power. Data values are normalized to 1 and mapped to colours linearly (**a**). Only one polarization component is injected into the fibre. The output signal is rapidly degraded into a complex periodic pattern (**b**). Both anticorrelated twin waves are injected. PDWs propagate in a symbiotic fashion, confirming the solitonic property of these kink entities. **c,** Output intensity profiles for an injected power of 23 dBm per polarization component. The polarization domains exhibit robust propagation on both orthogonal components (blue and red solid lines) when compared to the input signal (stars). In contrast, scalar propagation induces a high level of degradation (pink dashed line). Experimental results are compared with numerical simulations (triangles) and predicted PDW stationary solutions (circles) **d,** Correlation factor ρ between the input and output intensity profiles as a function of injected power. The single-component configuration (green circles) reveals a fast decrease of the correlation function, highlighting a strong degradation of the propagating wave. In contrast, PDWs (red triangles) preserve a correlation coefficient close to 1, confirming the high robustness and fidelity of the transmitted domains.

knots, they can be of any time duration and thus may be encoded individually to transmit optical data. In particular, as the signal is no longer periodic, a delayed replica is not sufficient to encode the initial twin waves. Hence, we used two parallel intensity modulators driven respectively by the *data* and *data* outputs of the PPG delivering a non-return-to-zero (NRZ) sequence. Both complementary waves are then properly synchronized and orthogonally recombined in such a way as to create the desired PDW sequence. To illustrate the principle, a 40 bit ASCII sequence encoding the acronym of our European Research Council (ERC) project PETAL was written at a repetition rate of 10 Gbit s^{-1}. Note that the data are encapsulated between two extended pre- and post-domains (6 bits) to avoid any impairments on the single edges of the sequence. The encoded PDWs propagate in a first 25-km-long reel of TrueWave fibre before being reamplified and injected in a second span of 25 km.

Figure 3a shows the PETAL sequence, monitored after 50 km of propagation, as a function of the transmitted power when only one of the two twin waves is injected. In this case, we clearly observe a significant signal degradation, leading to a complete loss of data. These impairments simply result from the detrimental impact of chromatic dispersion and self-phase modulation. In contrast, when both twin waves propagate simultaneously (Fig. 3b), we can clearly observe that the energy remains efficiently locked within each well-defined temporal region (see Supplementary Movie for direct laboratory observation). More specifically, as can be seen in the time domain for an injected power of 24 dBm (Fig. 3c), the PETAL sequence and its anticorrelated replica (red and blue) are ideally preserved after 50 km of propagation, unlike the single-component configuration (green), for which we observe a complete loss of the transmitted information. These observations confirm the capacity of PDWs to be addressed individually as well as the solitary nature of such kink structures.

Another experimental signature that corroborates the formation of PDWs is provided by spectral measurements. When only one polarization component propagates in the fibre (Fig. 3d, top), the sharp edges in the temporal profile of the initial signal are subjected to a strong self-phase modulation effect. This nonlinear process induces a large amount of chirp characterized by the generation of new frequencies and large spectral broadening. In contrast, thanks to their anticorrelated nature, the PDWs provide an almost ideal chirp compensation between interlocked components, which prevents significant spectral broadening (Fig. 3d, bottom). Note that we have also performed a 20 Gbit s^{-1} PDW transmission experiment involving a pseudo-random bit sequence in a 10-km-long fibre, the analysis of which reveals a well-opened eye-diagram (see section II.A in the Supplementary Information). These measurements clearly highlight the ability of PDWs to go beyond the limitations imposed by the nonlinear Kerr effect in normally dispersive fibres.

Polarization segregation phenomenon

To further highlight the robustness and robust properties of PDWs, we explored their spontaneous emergence from an incoherent system of random waves. To this end, the initial signal now consists of an unpolarized noise source composed of two uncorrelated and orthogonally polarized 10 GHz incoherent waves (see Methods). This signal is amplified before injection into a 10-km-long span of TrueWave fibre. At the output of the fibre, both orthogonal polarization components are separated by a PBS and characterized in the time domain by a 33 GHz bandwidth real-time oscilloscope. Figure 4a illustrates the temporal profiles of the initial signal recorded on both polarization components. We cannot observe any mutual correlation between the random waves. In contrast, after propagating in the 10-km-long optical fibre with an average power of 31 dBm, we can clearly notice in the snapshot of Fig. 4b
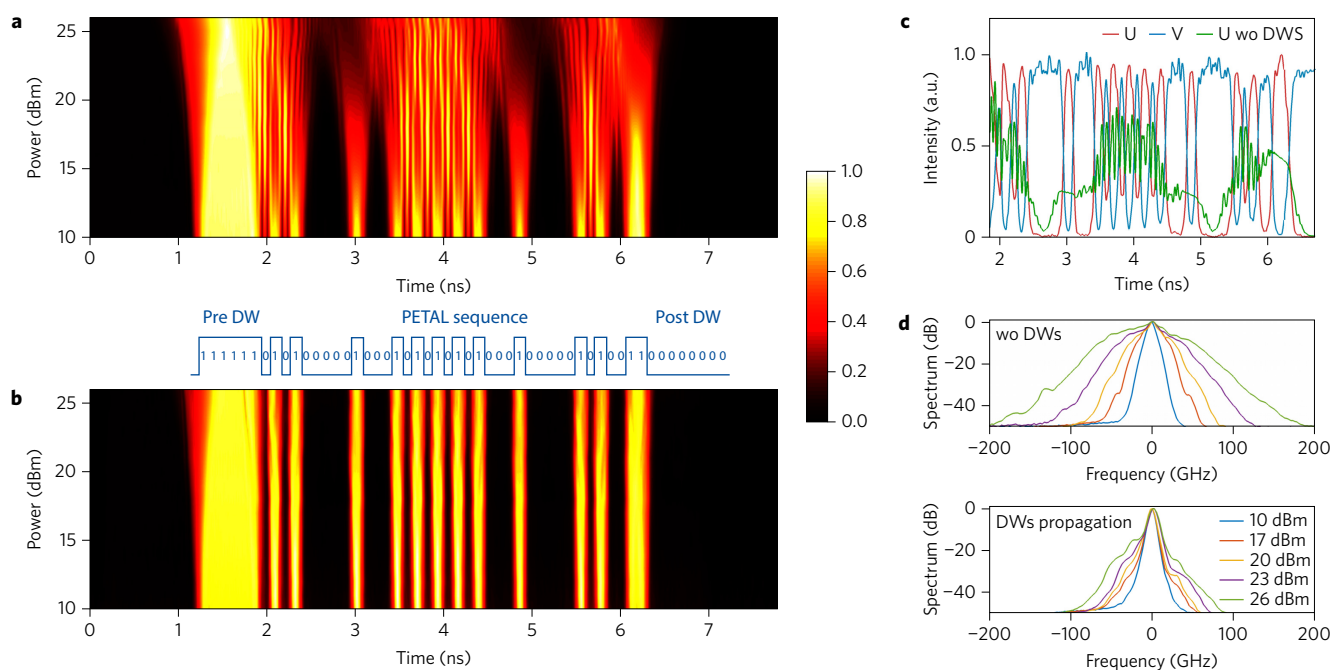
Figure 3 | Experimental data transmission through PDWs. a,b, Pseudo-colour plot made up of a vertical concatenation of the intensity profiles of the 10 Gbit s^{-1} PETAL sequence as a function of transmitted power after 50 km of propagation. Data values are normalized from 0 to 1 and are linearly mapped onto the full colour range. In **a**, only one polarization component is injected into the fibre, and the data sequence is degraded rapidly. In **b**, with PDW transmission, the sequence remains ideally preserved. **c,** Intensity profiles monitored at the output of the fibre for an injected power of 24 dBm. The signal and its anticorrelated replica are well conserved after 50 km of propagation, while the single-component configuration results (green solid line) are fully degraded (see Supplementary Movie for a direct laboratory observation). **d,** Output optical spectrum as a function of injected power. Top: only one single polarization component propagates. The initial signal is therefore subject to a strong self-phase modulation effect, inducing large spectral broadening. Bottom: both twin waves propagate. The PDWs are characterized by exact chirp compensation at the interface of each domain, preventing them from large spectral broadening.

the emergence of a mutual anticorrelation as well as an outstanding synchronization, which reflect a process of segregation among the orthogonal polarization components. This phenomenon results from the spontaneous emergence of definite temporal regions of polarized domains interconnected by DW structures.

To further assess whether a segregation process spontaneously occurs in this system of random waves, we computed the cross-correlation function μ_{dw} between the orthogonal polarization components. Note that (as described by the definition given in the Methods) a negative value of μ_{dw} indicates an anticorrelation, where when one of the polarization components increases, the corresponding orthogonal one decreases, and vice versa. Figure 4c presents a comparison between the input and output cross-correlation traces and confirms the foreseen results. Indeed, the original correlation (black) remains roughly flat and does not reveal any correlated temporal structure. In contrast, when monitored at the output of the fibre (green), we can clearly note a narrow spike centred on the null delay, characterized by a temporal width of 40 ps. Such a dip is a signature of the emergence of an anticorrelation among the polarization components, a feature that confirms the spontaneous formation of temporal domains of polarization.

From a broader perspective, this effect of self-organization can be interpreted as a fundamental phenomenon of phase segregation among the orthogonal polarization components. In this sense, it is in complete analogy with different forms of phase transitions in nature, such as the phase segregation of binary fluids[4] or the ferromagnetic order–disorder phase transitions in magnetic systems, as in spinor Bose–Einstein condensates[3]. More precisely, the segregation efficiency of our system can be characterized by the 'order parameter', the cross-correlation factor μ_{dw} (see Methods). Figure 4d reports the results of numerical simulations obtained for our experimental

configuration as a function of the total Hamiltonian H, related to the initial degree of incoherence (disorder) of the waves. In analogy with ferromagnetic materials, H plays the role of the temperature T in the microcanonical statistical optical ensemble considered here. We observe in Fig. 4d that there is a critical value of the Hamiltonian, H_c (T_c), around 0.005, below which the system is cold enough to exhibit a polarization segregation process. Above the transition, $H > H_c$, the system becomes too hot to exhibit such a self-ordering phenomenon. This behaviour is similar to the ferromagnetic transition in spin systems: by decreasing H, the system undergoes a transition from a disordered paramagnetic phase (unpolarized, $\mu_{dw} = 0$) towards an ordered ferromagnetic phase characterized by well-defined magnetic domains (PDWs formation $\mu_{dw} \neq 0$). The experimental results corresponding to PDWs transmission (Fig. 2, coolest state) as well as the 10 GHz incoherent wave propagation of Fig. 4 (higher temperature) are highlighted by stars in Fig. 4d and show good agreement with our numerical simulations.

Discussion

Our study provides clear experimental evidence of PDWs propagation in conventional telecom optical fibres. We first injected two anticorrelated orthogonal replicas of a fast square-shaped pulse train for which the strong nonlinear coupling induced at the boundaries of both twin waves acts as a powerful resilience strength to counter-balance the normally dispersive and nonlinear defocusing regime. This strong equilibrium allows the energy to be trapped in well-defined polarization domains, leading to the undistorted propagation of a 28 GHz train of PDWs along a 10-km-long normally dispersive optical fibre. We have also exploited their solitonic properties to establish a 10 Gbit s^{-1} data transmission beyond the nonlinear Kerr-induced limitations usually imposed in classical
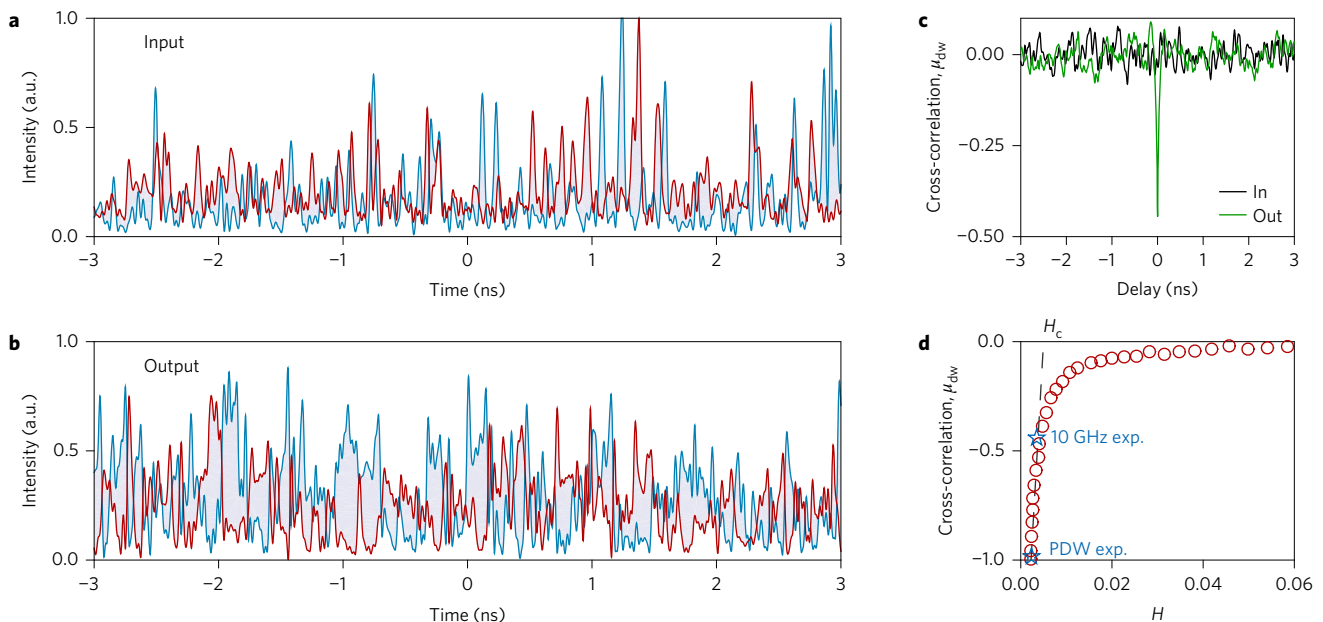
Figure 4 | Polarization segregation phenomenon. a, Experimental intensity profile of both orthogonally polarized partially incoherent waves recorded at the input of the fibre for a power of 31 dBm. **b**, Corresponding temporal profiles monitored at the output of the fibre. We can observe the emergence of an anticorrelation resulting from the spontaneous emergence of polarization domains, leading to a phenomenon of polarization segregation. **c**, Experimental cross-correlation function between orthogonal components of the signal calculated at the input (black) and output (green) of the fibre for an average power of 31 dBm. The narrow singularity at zero delay of the output cross-correlation μ_{dw} ($\tau = 0$) is a signature of the spontaneous emergence of polarization domains in this system of incoherent waves. **d**, Numerical segregation curves: cross-correlation factor μ_{dw} as a function of H (temperature). Below some critical value ($H < H_c$), the system undergoes a transition to segregation characterized by an anticorrelation ($\mu_{dw} < 0$) reflecting the spontaneous formation of DWs, in analogy with ferromagnetic materials. Experimental results corresponding to Fig. 2 (PDW exp.) and **b** (10 GHz exp.) are indicated by blue stars.

optical fibres. More fundamentally, we have confirmed the robust attractive nature of these entities, which manifest themselves by a remarkable phenomenon of polarization segregation, highlighted by the spontaneous emergence of polarized temporal domains in a system of incoherent random waves. This behaviour is interpreted in analogy with the ferromagnetic phase transition, in which a symmetry breaking occurs below a critical value of the energy, H_c (temperature), thus bringing the system towards an ordered phase of polarization domains characterized by a non-vanishing value of the order parameter μ_{dw}.

For practical applications, it is important to note that because PDWs are coupled due to an intensity-sensitive cross-polarization interaction, the phase of PDWs can also be encoded within each domain to increase the bit rate. Moreover, in contrast to classical bright scalar solitons, the topological nature of PDWs makes them robust with respect to external perturbations such as timing and amplitude jitter or differential group delay fluctuations. Therefore, their robust properties could find numerous applications in optical communications, high-power pulse propagation, all-optical processing, data storage and fibre lasers. The observation of polarization segregation could also find applications for the synchronization of chaotic oscillators and chaos-based optical data transmissions. Nevertheless, due to their anticorrelated nature, it is important to note that the orthogonal twin waves are carrying complementary, yet identical, intensity information, which could be a limitation for practical implementations.

It is important to stress that the present observation of PDWs in standard optical fibres goes against the commonly accepted opinion that the Manakov equations accurately model light propagation in random birefringent telecom fibres[35–38]. The Manakov model does not admit PDW soliton states, because the cross- and self-phase modulation coefficients coincide. Consequently, the present results raise important questions concerning the validity of the model for modern optical fibres and, more interestingly, our results open new

horizons towards the development of isotropic data transmissions. We ascribe the present observations to the fast spinning process imposed on modern manufactured fibres, where complex and rapid spin profiles, such as homogeneous or sinusoidal spinning, lead to an effective cancelling of residual birefringence[39–45]. This spinning effect then turns randomly birefringent fibres into a new type of fibre whose behaviour and properties are at the frontier between the so far traditional Manakov fibres and isotropic-like fibres (see Methods), which allows for the existence of universal PDW propagation in any arbitrary polarization basis.

We should thus expect that PDWs transmission performance could be improved with off-spooled or straight-line installed fibres for which the residual birefringence induced by bending is minimized[39]. Furthermore, our results can easily be extended into the spatial domain in bimodal fibres for spatial-division multiplexing applications[46]. In this case, the propagating domains would manifest themselves by a rapid beating of energy between two modes, allowing the possibility to encode information on the modal components of the waves instead of their intensity profiles.

To conclude, more than 20 years after the theoretical prediction of PDWs by Haelterman and Sheppard[14], we have reported the first direct experimental demonstration of the existence of these fundamental entities and confirmed their solitonic nature. More generally, these results can be considered as the first experimental evidence of symbiotic self-organization processes in optical fibres and, more importantly, as the first kink-type soliton transmission in nonlinear fibre optics.

Methods

Methods and any associated references are available in the online version of the paper.

References

1. Weiss, P. L'hypothèse du champ moléculaire et la propriété ferromagnétique. *J. Phys. Rad.* **6,** 661–690 (1907).
2. Reichl, L. *A Modern Course in Statistical Physics* (Wiley-VCH, 2004).
3. Dauxois, T. & Peyrard, M. *Physics of Solitons* (Cambridge Univ. Press, 2010).
4. Stamper-Kurn, D. N. & Ueda, M. Spinor Bose gases: symmetries, magnetism, and quantum dynamics. *Rev. Mod. Phys.* **85,** 1191–1244 (2013).
5. Weinberg, S. *The Quantum Theory of Fields* Vol. 2 (Cambridge Univ. Press, 1995).
6. Parpia, D. Y., Tanner, B. K. & Lord, D. G. Direct optical observation of ferromagnetic domains. *Nature* **303,** 684–685 (1983).
7. Kosevich, A. M. in *Solitons* (eds Trullinger, S. E., Zakharov, V. E. & Pokrovsky, V. L.) Ch. 11 (Elsevier, 1986).
8. Unguris, J., Celotta, R. J. & Pierce, D. T. Observation of two different oscillation periods in the exchange coupling of Fe/Cr/Fe(100). *Phys. Rev. Lett.* **67,** 140–143 (1991).
9. Allwood, D. A. *et al.* Magnetic domain-wall logic. *Science* **309,** 1688–1692 (2005).
10. Parkin, S. S., Hayashi, M. & Thomas, L. Magnetic domain-wall racetrack memory. *Science* **320,** 190–194 (2008).
11. Currivan-Incorvia, J. A. *et al.* Logic circuit prototypes for three-terminal magnetic tunnel junctions with mobile domain walls. *Nat. Commun.* **7,** 10275 (2016).
12. Tetienne, J. P. *et al.* The nature of domain walls in ultrathin ferromagnets revealed by scanning nanomagnetometry. *Nat. Commun.* **6,** 6733 (2015).
13. Haelterman, M. & Sheppard, A. P. Bifurcation of the dark soliton and polarization domain walls in nonlinear dispersive media. *Phys. Rev E* **49,** 4512–4518 (1994).
14. Haelterman, M. & Sheppard, A. P. Vector soliton associated with polarization modulational instability in the normal-dispersion regime. *Phys. Rev E* **49,** 3389–3399 (1994).
15. Malomed, B. A. Optical domain walls. *Phys. Rev. E* **50,** 1565–1571 (1994).
16. Sheppard, A. P. & Haelterman, M. Polarization-domain solitary waves of circular symmetry in Kerr media. *Opt. Lett.* **19,** 859–861 (1994).
17. Berkhoer, A. L. & Zakharov, V. E. Self-excitation of waves with different polarizations in nonlinear media. *Sov. Phys. JETP* **31,** 486–490 (1970).
18. Haelterman, M. Polarisation domain wall solitary waves for optical fibre transmission. *Electron. Lett.* **30,** 1510–1511 (1994).
19. Haelterman, M. Colour domain wall solitary waves for nonreturn-to-zero transmission scheme. *Electron. Lett.* **31,** 741–742 (1994).
20. Wabnitz, S. Cross-polarization modulation domain wall solitons for WDM signals in birefringent optical fibers. *IEEE Photon. Technol. Lett.* **21,** 875–877 (2009).
21. Gordon, J. P. & Haus, H. A. Random walk of coherently amplified solitons in optical fiber transmission. *Opt. Lett.* **11,** 665–667 (1986).
22. Kockaert, P., Haelterman, M., Pitois, S. & Millot, G. Isotropic polarization modulational instability and domain walls in spun fibers. *Appl. Phys. Lett.* **75,** 2873–2875 (1999).
23. Gutty, F. *et al.* Generation and characterization of 0.6-THz polarization domain-wall trains in an ultralow-birefringence spun fiber. *Opt. Lett.* **24,** 1389–1391 (1999).
24. Quinton, L. W. & Roy, R. Fast polarization dynamics of an erbium-doped fiber ring laser. *Opt. Lett.* **21,** 1478–1480 (1996).
25. Williams, Q. L., García-Ojalvo, J. & Roy, R. Fast intracavity polarization dynamics of an erbium-doped fiber ring laser: inclusion of stochastic effects. *Phys. Rev. A* **55,** 2376–2386 (1997).
26. Zhang, H., Tang, D. Y., Zhao, L. M. & Wu, X. Observation of polarization domain wall solitons in weakly birefringent cavity fiber lasers. *Phys. Rev. B* **80,** 052302 (2009).
27. Lecaplain, C., Grelu, P. & Wabnitz, S. Polarization-domain-wall complexes in fiber lasers. *J. Opt. Soc. Am. B* **30,** 211–218 (2013).
28. Marconi, M., Javaloyes, J., Barland, S., Balle, S. & Giudici, M. Vectorial dissipative solitons in vertical-cavity surface-emitting lasers with delays. *Nat. Photon.* **9,** 450–455 (2015).
29. Jang, J. K., Erkintalo, M., Coen, S. & Murdoch, S. Temporal tweezing of light through the trapping and manipulation of temporal cavity solitons. *Nat. Commun.* **6,** 7370 (2015).
30. Tsatourian, V. *et al.* Polarisation dynamics of vector soliton molecules in mode locked fibre laser. *Sci. Rep.* **3,** 3154 (2013).
31. Tomlinson, W. J., Stolen, R. H. & Johnson, A. M. Optical wave breaking of pulses in nonlinear optical fibers. *Opt. Lett.* **10,** 467–469 (1985).
32. Rothenberg, J. E. & Grischkowsky, D. Observation of the formation of an optical intensity shock and wave breaking in the nonlinear propagation of pulses in optical fibers. *Phys. Rev. Lett.* **62,** 531–534 (1989).
33. Fatome, J. *et al.* Observation of optical undular bores in multiple four-wave mixing fibers. *Phys. Rev. X* **4,** 021022 (2014).
34. Gilles, M. *et al.* Data transmission through polarization domain walls in standard telecom optical fibers. In *Spatiotemporal Complexity in Nonlinear Optics (SCNO)* (IEEE, 2015).
35. Pitois, S., Millot, G. & Wabnitz, S. Polarization domain wall solitons with counterpropagating laser beams. *Phys. Rev. Lett.* **81,** 1409–1412 (1998).
36. Manakov, S. V. On the theory of two dimensional stationary self-focusing of electromagnetic waves. *Sov. Phys. JETP* **38,** 248–253 (1974).
37. Wai, P. K. A. & Menyuk, C. R. Polarization mode dispersion, decorrelation, and diffusion in optical fibers with randomly varying birefringence. *IEEE J. Lightw. Technol.* **14,** 148–157 (1996).
38. Marcuse, D., Menyuk, C. R. & Wai, P. K. A. Application of the Manakov–PMD equation to studies of signal propagation in optical fibers with randomly varying birefringence. *IEEE J. Lightw. Technol.* **15,** 1735–1746 (1997).
39. Geisler, T. Low PMD transmission fibers. In *European Conference on Optical Communications (ECOC)* (IEEE, 2006).
40. Barlow, A. J., Ramskov-Hansen, J. J. & Payne, D. N. Birefringence and polarization mode-dispersion in spun singlemode fibers. *Appl. Opt.* **20,** 2962–2968 (1981).
41. Li, M. J. & Nolan, D. A. Fiber spin-profile designs for producing fibers with low polarization mode dispersion. *Opt. Lett.* **23,** 1659–1661 (1998).
42. Palmieri, L. Polarization properties of spun single-mode fibers. *IEEE J. Lightw. Technol.* **24,** 4075–4088 (2006).
43. Galtarossa, A., Palmieri, L. & Sarchi, D. Measure of spin period in randomly birefringent low-PMD fibers. *IEEE Photon. Technol. Lett.* **16,** 1131–1133 (2004).
44. Nolan, D. A., Chin, X. & Li, M. J. Fibers with low polarization-mode dispersion. *IEEE J. Lightw. Technol.* **22,** 1066–1088 (2004).
45. Palmieri, L., Geisler, T. & Galtarossa, A. Effects of spin process on birefringence strength of single-mode fibers. *Opt. Express* **20,** 1–6 (2012).
46. Pitois, S., Millot, G., Grelu, P. & Haelterman, M. Generation of optical domain-wall structures from modulational instability in a bimodal fiber. *Phys. Rev E* **60,** 994–1000 (1999).

Author contributions

J.F., P-Y.B. and M.Gi. performed the experiments. M.Gu., J.G. and A.P. contributed to the theoretical and numerical analysis. All authors participated in analysis of the results. J.F. wrote the paper and supervised the project.

Additional information

Supplementary information is available in the online version of the paper. Reprints and permissions information is available online at www.nature.com/reprints. Correspondence and requests for materials should be addressed to J.F.

Competing financial interests

The authors declare no competing financial interests.

Methods

Experimental set-up. All the experimental implementations were composed of standard off-the-shelf telecom fibres and components. The set-up involved in the propagation of the 28 GHz periodic train of PDWs consisted of an external cavity laser (Yenista, TLS) emitting a continuous wave (c.w.) centred at $\lambda = 1{,}555$ nm. This c.w. was first modulated by a phase modulator (PM) driven by a triple-tone radiofrequency (RF) signal (52, 203 and 506 MHz) to enlarge its spectral linewidth to push back the Brillouin scattering threshold of fibres under test high above the powers involved in the experiments. The c.w. was then encoded through a 40 GHz bandwidth intensity modulator (iXBlue Photonics), driven by a simple two-bit sequence of 0 and 1 at a bit rate of 28 Gbit s^{-1} provided by the electrical multiplexing of two NRZ PPGs (Anritsu). The resulting signal consisted of a train of 30 ps square-shaped pulses (fitted with a four-order super-Gaussian) at a repetition rate of 14 GHz (duty cycle of 1:2). The rise and fall time of these square pulses was measured as 8 ps. This pulse train was then injected at 45° to the axes of a polarization wave-shaper (2000S tunable liquid-crystal-based optical filter, Finisar), which, combined with a PBS, allowed us to successively duplicate and finely adjust the delay between the replicas by a half period and orthogonally polarization multiplex both complementary pulse trains. Both delayed orthogonal replicas thus appeared anticorrelated and consisted of a 28 GHz orthogonal polarization flip-flopping imposed on a c.w. This train of polarization kinks and antikinks structures was then amplified by an erbium-doped fibre amplifier (EDFA, 3S photonics). A polarization controller was used at the input of the fibre to adjust the input state of polarization (SOP). However, no influence of the input SOP was observed on the temporal profiles of the output signals. The PDWs were then injected into a 10-km-long TrueWave high-dispersion fibre (TWHD, commercially available from OFS). The fibre was characterized by a chromatic dispersion $D = -14.5$ ps nm^{-1} km^{-1} at 1,550 nm, a polarization mode dispersion of 0.02 ps km$^{-1/2}$, losses of 0.2 dB km^{-1} and a nonlinear Kerr coefficient $\gamma = 2.5$ W^{-1} km^{-1}. At the output of the system, both orthogonal replicas were polarization-demultiplexed by a polarization controller combined with a second PBS. This demultiplexing operation allowed us to decompose the output PDWs on the initial polarization basis to characterize both replicas in the time domain via a dual-input 70 GHz bandwidth photodiode (from u2t) and an electrical sampling oscilloscope (Keysight DCA). The 'initial polarization basis' refers to the basis recovered by switching off one polarization component at the input of the fibre and maximizing or minimizing the energy of the other component on one axis of the PBS at the system output.

Data transmission through PDWs. The phase-modulated c.w. was split into two arms using a polarization-maintaining 50:50 coupler. Both replicas were then intensity-modulated by two parallel intensity modulators (iXBlue Photonics). Each modulator was driven by the phase-matched *data* and *data* sequence delivered by the 10 Gbit s^{-1} NRZ PPG. Note that this PDW transmitter can be directly implemented using a high-bandwidth electro-optic polarization modulator. The emitted data sequence was chosen as the 40-bit-long ASCII code of the ERC project acronym PETAL (0101000001000101010101000100000101001100). The sequence was encapsulated between two extended polarization domains (6 bits of 0 on one arm and 6 bits of 1 on the other) to avoid any impairments on the single edges of the PETAL sequence. Both anticorrelated waves were then carefully synchronized in the time domain and orthogonally recombined in the 2000S polarization wave shaper. The encoded PDWs were then amplified by a 33 dBm EDFA and propagated in the first fibre spool of 25 km of TrueWave fibre before being reamplified by a second EDFA and injected into a second span of 25 km. At the output of the transmission line, the PDWs were characterized in the time domain using the same procedure as described in the previous section 'Experimental set-up'.

Polarization segregation phenomenon. The combination of anticorrelated pulse trains used to study PDW propagation was substituted by two uncorrelated incoherent waves. The injected signal consisted of amplified spontaneous noise emission (ASE) generated by an erbium-based optical source operating in the telecom C-band. This ASE signal was then sliced in the spectral domain with a 10 GHz bandwidth and simultaneously split into two orthogonal replicas by the 2000S polarization wave shaper. The resulting waves were then decorrelated in time by propagation in different fibres paths (1 km of SMF) and recombined with orthogonal polarizations by two polarization controllers and a PBS. Both incoherent waves were amplified by a 33 dBm EDFA (3S Photonics) before injection into a 10-km-long span of TrueWave fibre. At the output of the fibre, the orthogonal incoherent waves were polarization-demultiplexed using a polarization controller and PBS. As mentioned in the 'Experimental set-up' section, the initial polarization basis was finely retrieved by maximizing (minimizing) one or other polarization component on the output PBS in the absence (presence) of the second wave at the system input. To characterize the incoherent waves in the temporal domain, we directly monitored their intensity profiles by means of two finely balanced channels of a 33 GHz real-time oscilloscope associated with two 70 GHz bandwidth photodiodes (u2t).

Numerical modelling. There is some consensus that light propagation in randomly birefringent telecom fibres is accurately modelled by the set of Manakov equations[35–38]. In these coupled equations, the ratio between self- and cross-phase modulation

effects is unity, and the effective Kerr nonlinearity is reduced by a factor of 8/9 to take into account fast and random birefringence fluctuations, which lead to a homogeneous distribution of the polarization states on a Poincaré sphere. Nevertheless, as the formation of PDWs occurs when cross-phase modulation exceeds the self-phase modulation effect, a ratio between the cross- and self-phase modulation coefficients larger than 1 is required for their existence[13]. To provide an intuitive phenomenological description of our experimental observations, we implemented the following model, where u and v correspond to orthogonal polarization components of the field in an arbitrary polarization basis:

$$
\begin{cases}
i\dfrac{\partial u}{\partial z} = \dfrac{\beta_2}{2}\dfrac{\partial^2 u}{\partial t^2} - \gamma\left(|u|^2 + C_{\mathrm{XPM}}|v|^2\right)u \\[2mm]
i\dfrac{\partial v}{\partial z} = \dfrac{\beta_2}{2}\dfrac{\partial^2 v}{\partial t^2} - \gamma\left(|v|^2 + C_{\mathrm{XPM}}|u|^2\right)v
\end{cases}
\tag{1}
$$

where z corresponds to the propagation coordinate, t the local time in the reference frame of the fields, β_2 the chromatic dispersion coefficient (a normal dispersion regime is required for the existence of PDWs[13]), γ the Kerr coefficient and C_{XPM} the ratio between the cross- and self-phase modulation coefficients. Linear propagation losses have been neglected for simplicity. Note that, despite its apparent simplicity, this phenomenological model describes several properties of our experimental observations. In particular, it admits stable PDW solitons for $C_{\mathrm{XPM}} > 1$ and provides excellent agreement with the experimental results reported in Fig. 2c for a cross-phase modulation coefficient of $C_{\mathrm{XPM}} = 1.3$ and different choices of the experimental polarization basis.

These observations question the validity of the usual Manakov model commonly accepted to describe light propagation in standard telecom optical fibres. As will be discussed in the following, this unexpected finding results from the implementation of fast spinning profiles on the birefringence fibre axis during the drawing stage of the manufacturing process of modern spun fibres[39–45]. A commonly used spin profile has a sinusoidal shape, with the birefringence axes of the fibre rotating back and forth according to $\alpha(z) = \alpha_0\sin(2\pi z/L_{\mathrm{spin}}) + \eta(z)$, where the spatial period of the spinning process, L_{spin}, is the smallest spatial scale of the problem, typically of the order of few metres, while α_0, the amplitude of the spinning, can be as large as hundreds of rad m^{-1} (ref. 45). The stochastic contribution $\eta(z)$ is unavoidable because it originates in natural fibre birefringence fluctuations. The random function $\eta(z)$ has zero mean and is characterized by a correlation function $R(z/L_{\mathrm{c}})$, where L_{c} is the correlation length of the birefringence fluctuations. Note that the random contribution can be considered as a perturbation with respect to the imposed sinusoidal spinning, $\eta_0 = \sqrt{\langle\eta^2\rangle} \ll \alpha_0$. By using a homogenization theorem[47] and the Jacobi expansion $e^{2i\alpha_0\sin(2\pi z/L_{\mathrm{spin}})} = J_0(2\alpha_0) + \sum_{n=1}^{\infty} J_n(2\alpha_0)[e^{inkz} + (-1)^n e^{-inkz}]$, light propagation in the fibre can be shown to be described by the following reduced model:

$$
\begin{cases}
i\dfrac{\partial \tilde{u}}{\partial z} = \dfrac{\beta_2}{2}\dfrac{\partial^2 \tilde{u}}{\partial t^2} - \dfrac{\Delta\beta}{2}J_0(2\alpha_0)\tilde{v} + \varepsilon\tilde{u} - \dfrac{2\gamma}{3}\left(|\tilde{u}|^2 + 2|\tilde{v}|^2\right)\tilde{u} \\[2mm]
i\dfrac{\partial \tilde{v}}{\partial z} = \dfrac{\beta_2}{2}\dfrac{\partial^2 \tilde{v}}{\partial t^2} - \dfrac{\Delta\beta}{2}J_0(2\alpha_0)\tilde{u} - \varepsilon\tilde{v} - \dfrac{2\gamma}{3}\left(|\tilde{v}|^2 + 2|\tilde{u}|^2\right)\tilde{v}
\end{cases}
\tag{2}
$$

where $\tilde{u}$ and $\tilde{v}$ refer to circular polarization components of the field, $\Delta\beta$ is the propagation constant difference between the axes, $J_0(x)$ is the zeroth-order Bessel function of the first kind[44] and $\varepsilon(z) = \partial_z\eta(z)$ models the random contribution of the birefringence. As revealed by equation (2), the fast fibre spinning introduces a controlled polarization mode coupling through an effective beat length, $L_{\mathrm{B}}^{\mathrm{eff}} = 2/\left[\Delta\beta J_0(2\alpha_0)\right]$. In our experiments, the nonlinear and dispersive effects act in the km range, while the correlation length of polarization fluctuations ($L_{\mathrm{c}} \sim 50$ m) is typically much shorter than the effective beat length, $L_{\mathrm{c}} \ll L_{\mathrm{B}}^{\mathrm{eff}}$, with $L_{\mathrm{B}}^{\mathrm{eff}}$ of a few hundred metres. In this way, random birefringence fluctuations are essentially averaged out during the propagation. To properly understand such an averaging process, we follow the general procedure originally introduced by Wai and Menyuk[37] to describe the distribution of the Stokes vector of the optical field over the Poincaré sphere through analysis of the effective birefringence ($L_{\mathrm{B}}^{\mathrm{eff}}$) and random birefringence (L_{c}) effects. Making use of the diffusion approximation theorem[48], we derived a Fokker–Planck-like equation governing the evolution of the probability density of the Stokes vector on the surface of the Poincaré sphere. This equation reveals two fundamental limiting cases. First, when $\left(L_{\mathrm{B}}^{\mathrm{eff}}\right)^2/\left(\psi(\eta_0)L_{\mathrm{c}}\right) \ll L_{\mathrm{nl}}$, with $\psi(\eta_0) = 2\exp(-4\eta_0^2)\int_0^{\infty}\sinh^2\left(2\eta_0^2 R(s)\right)\mathrm{d}s$, then the Stokes vector becomes uniformly distributed over the Poincaré sphere before the onset of nonlinear effects. In this way, the averaging of the nonlinear terms leads to the usual Manakov system[37,38]. On the other hand, when $\left(L_{\mathrm{B}}^{\mathrm{eff}}\right)^2/\left(\psi(\eta_0)L_{\mathrm{c}}\right) \gg L_{\mathrm{nl}}$, it is possible to show that the optical field is governed by a set of equations formally analogous to those of a low birefringent (or isotropic) fibre, with an effective birefringence length, $L_{\mathrm{B}}^{\mathrm{eff}}\exp(2\eta_0^2)$. Our experimental observations place modern manufactured optical fibres between these two limits. Unfortunately, the evolution of the optical field in this intermediate regime cannot be described by deterministic equations, but by a set of coupled stochastic nonlinear Schrödinger equations. We have also studied the robustness of such reduced averaged equations with respect to noise perturbations. The analysis revealed that, thanks to the fast spinning of the fibre birefringence axes, noise fluctuations of velocity matching between the orthogonal polarization

components can be completely averaged out, which has the effect of dramatically reducing the detrimental impact of group-delay noise on signal propagation. See Supplementary Information for a detailed discussion of the theoretical developments.

Hamiltonian properties. The system of equation (1) conserves several important quantities, the power of each wave, $N_j = \int |j|^2 dt$, $j = u,v$, and the Hamiltonian $H = E + H_{nl} + H_{XPM}$, with the linear $E = \beta_2/2 \sum_{j=u,v} \int |\partial_t j|^2 dt$, nonlinear $H_{nl} = \gamma/2 \sum_{j=u,v} \int |j|^4 dt$ and interaction $H_{XPM} = C_{XPM} \gamma \int |u|^2 |v|^2 dt$ energy contributions. Note that in statistical mechanics, the energy H usually provides a measure of the 'amount of excitation' in the system (temperature in ferromagnetic materials for instance). In the weakly nonlinear regime ($E \gg H_{nl, XPM}$), the energy per particle E/N provides an appropriate measure of the amount of incoherence, which is related to the normalized spectral bandwidth of the waves, in analogy with kinetic gas theory[49].

Stationary solutions. Because no analytical solution exists for the temporal profile of PDWs, we numerically computed the stationary solutions of equation (1) to compare them with our experimental results (Fig. 2c). To this end, a tangent-hyperbolic ansatz was numerically injected into the set of coupled equations (1). These equations were then resolved with a standard split-step Fourier algorithm on five nonlinear lengths L_{nl}, defined as $1/\gamma P$, where P is the total average power. The propagating intensity profiles on each polarization component were then temporally averaged along the whole fibre length while the resulting root square provided a new set of initial conditions for equation (1). This process was repeated until the optical fields converged to a PDW soliton stationary solution (typically 50 iterations).

Intercorrelation. To calculate the correlation coefficient ρ between the input and output signals in Fig. 2d, the intensity profiles of the input and output polarization components $U_{in} = |u_{in}(t)|^2$ and $U_{out} = |u_{out}(t)|^2$ were recorded on the oscilloscope and the linear correlation was computed using the expression

$$\rho(U_{in}, U_{out}) = \frac{\langle U_{in} U_{out} \rangle}{\sqrt{\langle U_{in}^2 \rangle \langle U_{out}^2 \rangle}} \quad (3)$$

where angle brackets denotes the temporal averaging over the intensity profile.

The correlation function reported in Fig. 4c denotes the cross-correlation among both output orthogonal polarization components $U(t) = |u_{out}|^2$ and $V(t) = |v_{out}|^2$:

$$\mu_{dw}(U, V)(\tau) = \frac{\langle U(t) V(t-\tau) \rangle - \langle U(t) V(t) \rangle}{\sqrt{\text{var}[U(t)] \, \text{var}[V(t)]}}$$

where var(x) denotes the variance of x. Note that the above correlators solely involve the intensities of the waves and that they are related to the general notion of second-order coherence theory of classical vector fields. It is important to notice that $\mu_{dw}(U,V) < 0$ reveals an anticorrelation, indicating that when U increases, V decreases (and vice versa). This type of correlation function has been used

recently, for instance to characterize the noise and wavelength correlation properties of an octave-spanning supercontinuum[50].

The numerical segregation curve reported in Fig. 4d was obtained through equation (1) by computing μ_{dw} for $\tau = 0$ after propagation throughout the fibre (output of the system) for different values of the Hamiltonian H, which is a conserved quantity during propagation. The value of H for each individual simulation was varied by considering different spectral bandwidths of the initial incoherent waves, the spectra of which are Gaussian-shaped with random spectral phases (the waves exhibit Gaussian statistics with temporal fluctuations that are statistically stationary in time). Accordingly, irrespective of the value of H, $\mu_{dw} = 0$ for the initial condition at $z = 0$. If $H < H_c$ ($H > H_c$), the segregation process (does not) takes place and $\mu_{dw} \neq 0$ ($\mu_{dw} = 0$) after propagation throughout the fibre. Small values of H were obtained by progressively adding a c.w. component in the incoherent wave so as to develop classical polarization modulational instability (PMI). Further decreasing the temperature of the waves was finally obtained by progressively seeding the MI process until injection of the theoretical stationary solutions of PDWs.

Thermodynamic approach and phase transition. The phenomenon of polarization segregation has a thermodynamic origin, in the sense that it is thermodynamically advantageous for the system to exhibit polarization segregation, because this entails an increase in the amount of disorder. This counterintuitive phenomenon can be interpreted by recalling that the soliton realizes the minimum of the energy (Hamiltonian). The system then relaxes towards the state of lowest energy, which allows the small-scale fluctuations to store the maximum amount of kinetic energy (that is, 'disorder'). Indeed, the linear (kinetic) energy E provides a natural measure of the amount of disorder[49]. During propagation, E increases ($\Delta E > 0$) at the expense of a reduction in the interaction energy ($\Delta H_{XPM} < 0$), while the total energy H is kept constant. Note, however, that the one-dimensional system considered here does not exhibit a genuine thermalization[49], so the segregation process occurs far from thermodynamic equilibrium.

Data availability. The data that support the plots within this Article and other findings of this study are available from the corresponding author upon reasonable request.

References

47. Kurzweil, J. & Jarník, J. Limit processes in ordinary differential equations. *J. Appl. Math. Phys.* **38**, 241–256 (1987).
48. Fouque, J. P., Garnier, J., Papanicolaou, G. & Solna, K. *Wave Propagation and Time Reversal in Randomly Layered Media* Ch. 6 (Springer, 2007).
49. Picozzi, A. *et al.* Optical wave turbulence: toward a unified nonequilibrium thermodynamic formulation of statistical nonlinear optics. *Phys. Rep.* **542**, 1–132 (2014).
50. Godin, T. *et al.* Real time noise and wavelength correlations in octave-spanning supercontinuum generation. *Opt. Express* **21**, 18452–18460 (2013).